

Microwave anisotropies from the Galactic halo

Mark Walker

School of Physics, University of Sydney, NSW 2006, Australia

✉

Australia Telescope National Facility, CSIRO

Michiko Ohishi and Masaki Mori

Institute of Cosmic-Ray Research, University of Tokyo, Kashiwa, Chiba 277-8582, Japan

ABSTRACT

Models in which a large fraction of the Galactic dark matter takes the form of cold gas clouds imply that there is thermal microwave emission from the Galactic dark halo. Such models can therefore be directly constrained by data on the microwave sky, and in particular the very sensitive observations of microwave anisotropies which are now being made. To this end we have computed the anisotropy power-spectrum expected for a Galactic dark halo made of cold, dense gas clouds, including the effects of clustering with a CDM-like mass spectrum of mini-halo substructure. The power-spectrum displays two peaks: one, at $l \sim 50$, is the Poisson noise for the mini-halos, and the second, much larger and at much higher l , is the Poisson noise of the individual clouds. Because it appears on small (milli-arcsecond) angular scales, where the instrumental sensitivity is inevitably very poor, the latter signal is not directly detectable. By contrast, clusters of cold gas clouds may contribute significantly to the observed anisotropies if their emission has a grey-body spectrum. In this case the peak fluctuation, at $l \sim 50$, amounts to $4/|\sin b| \mu\text{K}$ in the Rayleigh-Jeans limit, and is the dominant Galactic foreground between 40 and 80 GHz. It will be possible to constrain this foreground component using low-latitude data from the MAP satellite, providing that its spectrum conforms to a grey-body. If the spectrum is “dusty” there will be relatively little power at frequencies below the thermal peak, and in this case the predicted anisotropies are shown to be negligible.

Subject headings: cosmic microwave background — galaxies: halos — dark matter

1. Introduction

Studies of the microwave sky play a critical rôle in cosmology, and measurements of the degree-scale microwave anisotropies can provide tight constraints on the cosmological model (e.g. Hu and Dodelson 2002). It is therefore particularly important that we understand the power-spectrum arising from foreground microwave sources, and much attention has already been given to this topic (e.g. Tegmark and Efstathiou 1996; de Oliveira-Costa and Tegmark 1999). The various foreground sources which have been considered to date include: normal galaxies

and Active Galactic Nuclei; Galactic synchrotron emission; Galactic free-free emission; and Galactic dust emission. At frequencies in the range $50 \lesssim \nu \lesssim 150$ GHz, none of these sources is thought to make a significant contribution to the power-spectrum for multipoles $l \lesssim 500$ (Tegmark and Efstathiou 1996). This conclusion must be regarded as tentative in the case of the extragalactic sources, because the difficulty of undertaking large area surveys at high radio-frequencies means that the source populations are poorly constrained in this frequency range — see Toffolatti et al (1999) for a discussion. The Galactic emission, on the other hand, is known to be very significant at

both low frequencies (synchrotron) and high frequencies (dust); and, in fact, at all frequencies at low Galactic latitudes. However, observing at high/low frequencies yields template distributions for those contaminants, and these templates can be cross-correlated with data in the preferred frequency band to estimate their contamination level. This procedure has provided robust confirmation that, at high latitudes, the recognised Galactic foregrounds do not significantly contaminate the COBE DMR data (Kogut et al 1996).

Although robust, the method we have just described clearly cannot be applied if there is no template for the foreground. This is the circumstance we are faced with if the Galactic dark matter has a substantial component in the form of cold gas clouds, as has been proposed by a number of authors (Pfenniger, Combes and Martinet 1994; De Paolis et al 1995; Henriksen and Widrow 1995; Gerhard and Silk 1996; Walker and Wardle 1998; Sciamia 2000a). Such clouds emit primarily in the microwave band, and that emission is thermal at temperatures of only a few degrees; consequently the magnitude of this putative foreground is at present only subject to very weak direct observational constraints. Indirect constraints – from the small amplitude of fluctuations in the Cosmic Microwave Background (CMB), and from Big Bang Nucleosynthesis – are generally supposed to exclude any significant amount of baryonic dark matter (e.g. Turner and Tyson 1999), but these arguments are not entirely free of loopholes (Hogan 1993; Walker and Wardle 1999) and direct constraints are desirable. Given the great sensitivity of the microwave data which are now being acquired, it is therefore prudent to consider what Galactic microwave emission is expected for models in which the dark matter is composed of cold gas.

To proceed with a calculation we need to specify a particular model. The success of the now-standard structure formation paradigm, exemplified by the Cold Dark Matter model (e.g. Peebles 1992), argues that any acceptable model must possess clustering properties that are similar to those of CDM, in order to match the data on large-scale-structure, and consequently we utilise the properties of CDM halos as a guide. It then remains to specify the properties of the individual clouds. Radio-wave scintillation data – specif-

ically the Extreme Scattering Events (Fiedler et al 1987; Fiedler et al 1994) – suggest a vast population of \sim AU-sized clouds, each of planetary mass (Walker and Wardle 1998), and we assume that these properties are appropriate to the individual clouds.

The present paper is organised as follows: in §2 we derive the angular spectrum for an unclustered cloud distribution; in §3 the influence of CDM-like clustering is considered; §4 combines the results of §§2,3 into a prediction for the root-mean-square temperature anisotropy spectrum, under the assumption of grey-body emission, and considers the constraints which existing data place upon the input model; §5 then considers how these results are modified in the case where the clouds have “dusty” emission spectra.

2. Power from individual clouds

As a tool to describe the statistical properties of the microwave sky, it is conventional to employ the power-spectrum

$$C_l \equiv \frac{1}{2l+1} \sum_{m=-l}^l a_{lm}^* a_{lm}, \quad (1)$$

where the a_{lm} are coefficients in the expansion of the brightness temperature field, δT , in terms of the spherical harmonic functions Y_{lm} :

$$\delta T(\theta, \phi) = \sum_{l=0}^{\infty} \sum_{m=-l}^l a_{lm} Y_{lm}(\theta, \phi). \quad (2)$$

We will model only the power-spectrum which would be derived from measurements over a small patch of sky, so that we need only consider the case $l \gg 1$, for which some mathematical simplifications are possible. The restriction to large l also means that we do not have to model the structure of the Galaxy in any detailed way, because we are considering angular scales which are sufficiently small that the source (cloud) positions are essentially random.

The starting point for our calculation is the white-noise spectrum ($C_l = C_l^w$, independent of l) which is introduced by a random distribution of point sources, each of flux F , with a mean number per unit solid-angle of $dN/d\Omega$:

$$C_l^w = F^2 \frac{dN}{d\Omega}. \quad (3)$$

If the individual sources are not point-like, but each source is axisymmetric with power-spectrum $F^2 C_l^s$ (so that C_l^s is the power-spectrum for a source of unit flux), then the power-spectrum of the source population is $C_l = 4\pi C_l^s C_l^w$. Now if we consider sources at various distances, D , with corresponding number density n , it follows that $\delta(dN/d\Omega) = D^2 n \delta D$, and hence

$$\frac{dC_l}{dD} = 4\pi C_l^s D^2 n F^2. \quad (4)$$

Integrating along the line-of-sight then yields the power-spectrum of this source population.

The gas clouds we are considering are expected to cool primarily through thermal continuum emission in the microwave band, with this emission arising from precipitates of molecular hydrogen (Wardle and Walker 1999). The bulk of the interior of a cloud is too hot for solid hydrogen to exist; all the radiation is expected to come from a thin, nearly isothermal atmosphere. There is at present no quantitative description of the internal cloud structure, and consequently we have adopted a simple model of the surface brightness profile, namely a uniform intensity disk. Provided that the cloud radius is $R_o \ll D$, this model yields a power-spectrum

$$C_l^s = \frac{1}{4\pi} \left[\frac{2 J_1(lR_o/D)}{lR_o/D} \right]^2 \quad (5)$$

for a single cloud, with J_1 being a Bessel function of the first kind. For $l \gg D/R_o$ this model is a poor one in that it over-predicts the power spectrum — a result of the discontinuity in the intensity profile at the limb of the cloud. To counteract this tendency to overpredict the power at large l , we have simply truncated the power spectrum at $lR_o = 10D$. This ad hoc treatment of the high frequency behaviour means that the predicted power-spectrum for the cloud population is unreliable in the regime $lR_o \gg \langle D \rangle$; however the corresponding angular scales are so small (sub-milli-arcsecond; see §4) that this limitation is not important in practice.

In equilibrium the luminosity of any cloud must be balanced by heating, so a cloud of mass M_o satisfies $\Gamma M_o = 4\pi D^2 F$, where Γ is the heating rate per unit mass. This heating is expected to be due primarily to cosmic-rays (Wardle and Walker 1999; Sciama 2000a). In this paper we consider

only lines-of-sight at high or mid Galactic latitude, and for these directions it is reasonable to model the cosmic-ray density variations with a simple analytic function; we employ the form $\Gamma = \Gamma_0 \exp(-|z|/h)$, where $z = D \sin b$ is the height above the Galactic disk at Galactic latitude b . A more realistic model is offered by a sum of thin and thick disks (Higdon 1979; Beuermann, Kanbach and Berkhuijsen 1985), but for our illustrative calculations this level of detail is unwarranted and we have adopted a single component model, with a scale-height of $h = 3$ kpc (corresponding to the thick disk). This choice of scale-height is a compromise between the (larger) values deduced from analysis of the radio synchrotron data (Higdon 1979; Beuermann, Kanbach and Berkhuijsen 1985), and the (smaller) values inferred from existing cosmic-ray propagation models (Webber, Lee and Gupta 1992). Note, however, that if the putative cloud population does indeed exist, then these models of cosmic-ray propagation need to be revised (Sciama 2000a, b).

To complete our prescription we need to specify the number density of the clouds. For this purpose we employ the collisional isothermal halo model of Walker (1999: W99). In this model, or indeed any quasi-spherical halo model, the density of dark matter varies only slowly in comparison to the scale-height of the cosmic-ray disk, and this variation can be neglected:

$$n = \frac{\rho}{M_o} \simeq \frac{V^2}{4\pi G M_o (r_{gc}^2 + r_d^2)}, \quad (6)$$

where $V \simeq 220$ km s⁻¹ is the rotation speed for the Galactic disk, $r_{gc} \simeq 8.5$ kpc is the distance to the Galactic Centre, and r_d is the core radius of the dark halo. For the Galaxy, the latter is specified as $r_d \simeq 6.2$ kpc in W99's model.

For a homogeneous source population, with $n \simeq$ constant, and $F \propto 1/D^2$, equation 4 indicates that the low-frequency power (for which $4\pi C_l^s \simeq 1$) is dominated by the nearest clouds within the field-of-view, $\Delta\Omega$. The lower limit on the integration over D must therefore not be taken as zero, but as D_{min} , the expected distance of the closest cloud, with

$$\frac{\Delta\Omega}{3} D_{min}^3 n := \frac{1}{2}. \quad (7)$$

For a field of $\Delta\Omega \sim 0.1$ sr, similar to the coverage

of the BOOMERanG experiment (de Bernardis et al 2000), for example, we have $D_{min} \simeq 0.57$ pc.

Using the descriptions given above, we can compute the power-spectrum for our model of unclustered gas clouds, C_l^u :

$$\frac{C_l^u(k)}{C_l^u(0)} = y \int_y^\infty dx \exp(-x|\sin b|) \left[\frac{2J_1(k/x)}{k} \right]^2, \quad (8)$$

where $x \equiv 2D/h$, so that $y = 2D_{min}/h$, and $k \equiv 2lR_o/h$. The power level at zero frequency is

$$C_l^u(0) = \frac{M_o V^2 \Gamma_0^2}{(4\pi)^3 G(r_{gc}^2 + r_d^2) D_{min}}. \quad (9)$$

Figure 1 shows a plot of $\delta I = k \sqrt{C_l^u(k)/C_l^u(0)}$, the standard-deviation of the intensity fluctuations. In constructing this figure we have taken $|\sin b| = 1$, and we have adopted the parameters of the model given above, for which $D_{min} \simeq 0.57$ pc, hence $y \simeq 3.8 \times 10^{-4}$.

Three distinct regimes of behaviour can be seen in figure 1. For $k \ll y$, all of the clouds are expected to be unresolved on the corresponding angular scales, so the power-spectrum is simply $C_l^u(k) \simeq C_l^u(0)$ and the r.m.s. intensity fluctuations are proportional to k . For $k \sim y$ some of the closest clouds are resolved out, and for $y \ll k \ll 1/|\sin b|$ the power flattens to $C_l^u(k)/C_l^u(0) \simeq 2y/\pi k$, so the r.m.s. intensity is $\delta I \propto \sqrt{k}$. It should be noted that up to this point the results are independent of the scale-height, h , and the line-of-sight, i.e. the latitude b ; in other words the behaviour is completely determined by the local conditions (dark matter density and cosmic-ray heating rate). However, the location ($k = k_p \simeq \sqrt{2}/|\sin b|$) and height of the peak fluctuations are influenced by h and b : clouds which lie outside the cosmic-ray disk have very low luminosity and consequently contribute little to the temperature anisotropies, so on angular scales smaller than those characteristic of a cloud at distance $D \sim h/|\sin b|$ the fluctuations decline rapidly. The peak value of the anisotropy spectrum can be estimated from $C_l^u(k_p)/C_l^u(0) \simeq \sqrt{2}y|\sin b|/\pi$. If we make numerical estimates of these values we find that the peak occurs on milli-arcsecond scales ($l \sim 3 \times 10^8$) and reaches a value ~ 4 mK, as discussed in §4.

2.1. Source counts

In connecting the foregoing model with observations we must take a little care, in that low-frequency power is dominated by the brightest sources within the field-of-view. If observations are made with a sensitive instrument that has good angular resolution, then these will be recognised as point sources and subtracted from the map before the anisotropy power-spectrum is estimated. In order to quantify this possibility we need to estimate the source counts. For bright sources, with $D \ll h/|\sin b|$, the source luminosity and density are uniform over the population, hence the usual Euclidean result applies:

$$\frac{dN(> F)}{d\Omega} = \frac{1}{4\pi} \left(\frac{F_{max}}{F} \right)^{3/2}, \quad (10)$$

where F_{max} is the expected flux of the brightest source on the sky. For the case we are considering, the bolometric luminosity is ΓM_o , so the brightest source is expected to have a flux of $F_{max} = \Gamma M_o / 4\pi D_{min}^2$. This result breaks down at low flux levels, where the sources lie outside the cosmic-ray disk, but F_{max} corresponds to a source which is only about 0.1 pc distant, so with a disk scale-height of $h = 3$ kpc the form given in equation 10 is a good approximation for $F \gg 10^{-9} F_{max}$. Numerical estimates for F_{max} are given in §4.

2.2. Mean sky brightness

Using the foregoing model, it is straightforward to calculate the mean sky brightness contributed by the cloud population, the result is:

$$\langle I \rangle = \frac{\Gamma_0 V^2 h \csc|b|}{(4\pi)^2 G(r_{gc}^2 + r_d^2)}. \quad (11)$$

The mean sky brightness thus does not depend explicitly on the properties of the individual clouds, although there is an implicit dependence of Γ_0 on the column-density of the clouds, as we shall see in §4.1. Consequently the same result for $\langle I \rangle$ is obtained for the model described in the next section, in which clustering of the clouds is considered. Using the cosmic-ray heating rate determined in §4.1, and an atmospheric temperature of 4.2 K for the clouds (§4.2), we deduce a mean sky brightness temperature, in the Rayleigh-Jeans regime, of $\langle T_b \rangle \simeq 30 \mu\text{K}$ at the Galactic pole.

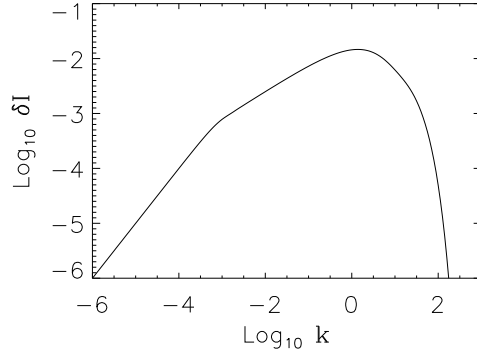


Fig. 1.— The root-mean-square intensity fluctuations, δI , due to a randomly distributed population of cold clouds, heated by cosmic-rays, as described by equation 8. This graph is appropriate for observations of a field of size $\Delta\Omega = 0.1$ sr near the Galactic pole ($|b| = 90^\circ$). The axes are scaled such that $k = 2lR_o/h$, and $\delta I = k\sqrt{C_l^u(k)/C_l^u(0)}$.

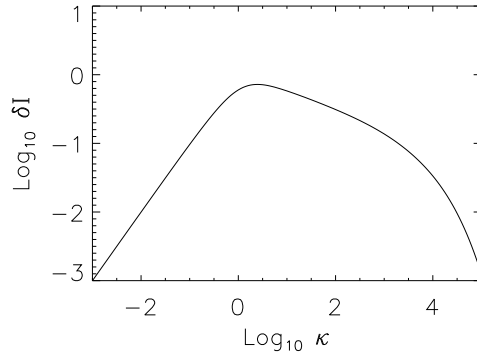


Fig. 2.— The root-mean-square intensity fluctuations, $\delta I = \kappa\sqrt{C_l^c(\kappa)/C_l^c(0)}$, due to a population of mini-halos with a CDM-like mass spectrum. This plot is appropriate to a survey region of size $\Delta\Omega = 0.1$ sr near the Galactic pole. At low frequencies ($\kappa \ll 1$) essentially all of the mini-halos are unresolved and $\delta I \simeq \kappa$, reaching a peak of $\delta I \simeq 1$ at $\kappa \simeq 1$. This peak reflects the characteristic angular size of the closest mini-halos, which is of order 4° .

3. Power due to clustering

The Cold Dark Matter model provides an elegant framework within which we can understand the formation of structure in the Universe (Blumenthal et al 1984; Davis et al 1985; Peebles 1992). The key ingredients of this model are (i) a scale-invariant power-spectrum of density fluctuations, and (ii) dark matter which initially has low velocities. Gravity does the rest. Dense gas clouds are expected to satisfy the second of these requirements (i.e. they are a type of cold dark matter), provided that they form in the early Universe and survive to the present time (Hogan 1993; Walker and Wardle 1999). The first requirement is naturally satisfied for inflationary models of the early Universe, independent of the nature of the dark matter. Consequently structures forming in a Universe dominated by dense gas clouds may resemble those found in CDM models. This is as true for galactic and sub-galactic mass-scales as it is for cluster and super-cluster scales. The sub-structure within CDM halos follows a power-law mass spectrum with index approximately equal to -2 (Moore et al 1999; Klypin et al 1999), and we adopt this result as our model for the clustering properties of dense gas clouds comprising the Galactic dark halo. Consequently we expect the halo to be populated with a number density n_{mh} of mini-halos, such that

$$\frac{dn_{mh}}{dM} = \frac{\rho}{M^2 \log_e(M_2/M_1)} \quad (12)$$

extending over a mass range $M_1 < M < M_2$. It should be noted that this formulation implies that *all* of the dark matter is in the form of mini-halos, and this is apparently at odds with the results of simulations, for which only $\sim 10\%$ of the halo mass appears in this form (e.g. Ghigna et al 1998). However, the simulations which have been undertaken to date are capable of resolving only the upper end of the mini-halo mass range which we consider here (see §4.3), and such simulations have little to say about the existence of lower mass halos. Moreover, if the only relevant physics is cold gravitational collapse, acting on a power-law spectrum of density perturbations, then there is no reason to expect any characteristic mass-scale in the clustering, until one reaches masses which are so small that the discreteness of the dark matter particles begins to play a role. At the very least

the circumstance described by equation (12) can be considered as a limiting case: the total density in mini-halos cannot exceed the total dark matter density.

Because these aggregates are much smaller than their parent halos, their internal structure has not yet been thoroughly investigated with simulations. However, we know that their density profiles are consistent with tidally-truncated isothermal spheres (Moore et al 1999), and we adopt that description. In addition to tidal truncation, the density distribution must have a central core as a result of collisions occurring between the constituent clouds (W99). We therefore employ a model density profile

$$\varrho = \frac{M \exp(-r^2/2r_t^2)}{(2\pi)^{3/2} r_t (r^2 + r_c^2)}, \quad (13)$$

where r_t is the tidal radius and r_c the core radius of the mini-halo, and we have assumed that $r_c \ll r_t$. From this three-dimensional profile we can determine the column-density seen by a distant observer. The microwave intensity is proportional to this column, so the angular power-spectrum for a source of unit flux is

$$C_l^s \simeq \frac{\exp(-2lr_c/D)}{4\pi + 8l^2 r_t^2 / D^2}. \quad (14)$$

The features of this power-spectrum are as follows. For $lr_t \ll D$, $C_l^s \simeq 1/4\pi$; and for $D/r_t \ll l \ll D/r_c$ we have $C_l \propto 1/l^2$, cutting off exponentially for $l \gtrsim D/r_c$. Most of the contribution to the intensity fluctuations therefore comes from the frequency range $D/r_t \ll l \ll D/r_c$, and the existence of a core in the density profile is critical in determining the power-spectrum at high wavenumbers. If there were no core in the halo density profile, the intensity fluctuations would be independent of l in the range $l \gg D/r_t$.

We need to calculate the tidal radius and the core radius; both depend on the mass of the mini-halo under consideration. To estimate the tidal radius we note that the scale-height of the cosmic-ray disk, h , is expected to be small in comparison with r_{gc} , so we can make the approximation that all of the mini-halos within the field-of-view which make a significant contribution to the power-spectrum are at the same Galactocentric radius $r = r_{gc}$. Now the tidal radius of each

mini-halo is determined by the tides at perigalacticon, and because r_{gc} is an upper limit to the galactocentric radius at that point – i.e. most mini-halos will be on orbits which take them much closer to the centre of the Galaxy – and simulations of halo formation find that mini-halo orbits have quite large eccentricities (Ghigna et al 1998), we take $r_{gc}/2$ as an estimate of the Galactocentric radius at perigalacticon. We then follow the usual procedure (Binney and Tremaine 1987), leading to an estimated tidal radius $r_t^3 := \alpha M$, where

$$\alpha = \frac{Gr_{gc}^2}{12V^2} \simeq 8.0 \times 10^{21} \text{ cm}^3 \text{ g}^{-1}. \quad (15)$$

The core radius of each halo is determined by the collisional nature of the dark matter (W99), with the velocity dispersion of each mini-halo being related to its mass by comparing equation 13 (for $r \ll r_t$) with the standard form for a self-gravitating isothermal sphere. This procedure leads to the estimate $r_c^2 = \gamma M$, where

$$\gamma = \frac{12\sqrt{2}Vt_H}{(2\pi)^{3/4}\pi\Sigma r_{gc}} \simeq 2.5 \text{ cm}^2 \text{ g}^{-1}, \quad (16)$$

with $t_H \simeq 10^{10}$ years being the elapsed time since the mini-halo virialised, and $\Sigma \equiv M_o/\pi R_o^2$ is the mean column-density of the individual clouds. W99’s model gives $\Sigma \simeq 140 \text{ g cm}^{-2}$, and we have used that value in estimating γ .

The power-spectrum for the whole population of mini-halos can be obtained by integrating

$$\frac{d^2 C_l}{dD dM} = 4\pi C_l^s D^2 \frac{dn_{mh}}{dM} F^2, \quad (17)$$

with respect to M and D . The integration over distance is taken out to infinity but, as for the case of the individual clouds, the lower limit cannot be taken as zero because at low frequencies the power-spectrum is dominated by contributions from the nearest sources. We can estimate the lower distance limit, as a function of mini-halo mass, by analogy with equation 7, making the replacement $n \mapsto \log_e(M_2/M_1)dn_{mh}/d\log_e M$, whence

$$\frac{\Delta\Omega}{3} D_{min}^3 \log_e(M_2/M_1) \frac{dn_{mh}}{d\log_e M} = \frac{1}{2}. \quad (18)$$

This equation states that the closest mini-halo within the mass range M_1 to M_2 has a 50% chance of being located within a distance D_{min} . If we

now define $z \equiv 2D_{min}/\tilde{h}$, where $\tilde{h} \equiv h/|\sin b|$ then with reference to the expected mini-halo mass spectrum (equation 12) we can write $z^3 := \beta M$, where

$$\beta = \frac{12}{\tilde{h}^3 \Delta\Omega \rho} \simeq 2.7 \times 10^{-40} \text{ g}^{-1}. \quad (19)$$

In estimating the numerical value of β , here, we have assumed a field-of-view of $\Delta\Omega = 0.1$ sr at the Galactic pole ($|\sin b| = 1$), with the mass limits $M_{1,2}$ as given in §4. An important point can now be made, even before we calculate the power-spectrum of the population. Because the tidal radius, r_t , and the distance to the closest mini-halo, D_{min} , both vary as $M^{1/3}$, the angular radius of the nearest mini-halo is $r_t/D_{min} = (2/\tilde{h})(\alpha/\beta)^{1/3} \sim 4^\circ$, independent of M , (and also independent of h and b). Remembering that the power-spectrum is dominated by contributions from the closest mini-halos, we thus expect a peak in the intensity fluctuations on degree scales.

We can now integrate equation 17 over D and M to obtain our power-spectrum estimate; the result is

$$C_l^c = C_l^c(0) \mathcal{I}(\kappa, \kappa_c), \quad (20)$$

where

$$C_l^c(0) = \frac{\Delta\Omega}{6 \log_e(M_2/M_1)} \left(\frac{V}{4\pi}\right)^4 \left[\frac{\Gamma_0 \tilde{h}}{G(r_{gc}^2 + r_d^2)} \right]^2, \quad (21)$$

and

$$\mathcal{I}(\kappa, \kappa_c) = 3 \int dz z^2 \int_z^\infty dx \frac{\exp(-x - \kappa z^{3/2}/\kappa_c x)}{x^2 + \kappa^2 z^2}, \quad (22)$$

having introduced $x \equiv 2D/\tilde{h}$. The wavenumber is now expressed as $\kappa \equiv (l/\tilde{h})(\alpha/\beta)^{1/3}(8/\pi)^{1/2}$, and the parameter κ_c is $\kappa_c := \alpha^{1/3}\beta^{1/6}/\sqrt{2\pi\gamma}$. The limits of integration over z are determined by the limits of the mini-halo mass-spectrum, so $z_{1,2}^3 := \beta M_{1,2}$, and we have adopted the values of $M_{1,2}$ as estimated in §4, leading to $z_1 = 3.8 \times 10^{-3}$ and $z_2 = 9.1$.

It is easy to verify that $\mathcal{I} \rightarrow 1$ as $\kappa \rightarrow 0$. Unfortunately this low frequency regime (i.e. $\kappa \ll 1$) is the only one for which we have been able to determine a simple analytic form for \mathcal{I} . It is, however, straightforward to evaluate \mathcal{I} numerically, once κ_c is specified. Using the numerical values for the various parameters which we have already given

(see also the following section), we find $\kappa_c \simeq 1.3$, leading to the fluctuation spectrum shown in figure 2. At low frequencies, where essentially all of the mini-halos are unresolved, this spectrum displays the usual form for Poisson noise from point-like sources: $\delta I \propto \kappa$. The spectrum then peaks at $\kappa \sim 1$, corresponding to the characteristic angular scale of the nearest mini-halos, and declines slowly as κ increases.

4. Model parameters

The anisotropy models we have just presented do not incorporate any free parameters: all of the various inputs can be estimated – albeit rather crudely in some cases – from other types of data. We now turn to the business of estimating those quantities which have not yet been specified, in order to arrive at numerical results for the brightness-temperature anisotropy spectrum.

4.1. Cosmic-ray heating

For high column-density clouds, such as we are considering here ($\Sigma \simeq 140 \text{ g cm}^{-2}$, W99), there is significant attenuation of the cosmic-ray flux from surface to centre, and so the cosmic-ray heating rate differs from that deduced for diffuse interstellar gas (Umebayashi and Nakano 1981; Sciamia 2000a). We have estimated the cosmic-ray heating rate local to the Sun, Γ_0 , appropriate to dense clouds, using the Monte Carlo simulation program GEANT (Ohishi, Mori and Walker 2003; <http://wwwinfo.cern.ch/asd/geant>). GEANT was developed for studying interactions in laboratory particle detectors, but can be used for astrophysical calculations without modification. By using GEANT we are able to study the transport of cosmic rays into high column-density clouds, with all relevant particle interactions included. The main disadvantage of GEANT, for our purposes, is that it does not conserve energy very accurately in the hadronic interactions (GEANT Bug Reports #171 & #389). There is a “patch” available for the relevant piece of code, GHEISHA which treats hadronic interactions, but this patch appears to introduce further problems of its own (GEANT Bug Report #415), and we have therefore used GEANT with the un-patched version of GHEISHA. We can easily calculate the heating rate in the limiting case of very dense clouds,

without using GEANT, because all of the incident power is absorbed in this case. We find that in this limit GEANT over-estimates the power deposition by $\sim 25\%$, and this estimate can be taken as a gauge of the accuracy of our computations of the heating rate, Γ .

For the purposes of estimating the microwave emissivity of the gas, we need only calculate the total power deposited by the incident cosmic-rays; however, the interaction between the cosmic-rays and the gas also gives rise to gamma-rays (principally via electron bremsstrahlung and π^0 production), and we will report elsewhere on the consequences of these processes for the interpretation of the mean gamma-ray spectrum of diffuse Galactic emission (Ohishi, Mori and Walker 2003), and for the interpretation of the unidentified EGRET sources (Walker, Mori and Ohishi 2003). In our calculations of the gas heating rate we approximated each cloud as a sphere of uniform density, and used GEANT to compute the power deposited as a function of the gas density (the radius of each cloud being fixed at 1 AU). We adopted the “median” cosmic-ray proton spectrum quoted by Mori (1997; but note that the units on his equation [3] should read $\text{cm}^{-2}\text{s}^{-1}\text{sr}^{-1}\text{GeV}^{-1}$), including energies down to 100 MeV, and the electron spectrum from Skibo and Ramaty (1993), with a low-energy cutoff of 10 MeV; more details of these simulations will be presented elsewhere (Ohishi, Mori and Walker 2003). These cosmic-ray spectra are appropriate to the vicinity of the Sun, and it is implicit in our model that the spectra elsewhere in the Galaxy have the same shape, and differ only in normalisation. We caution that the cosmic-ray spectra which we are employing are not identical to the spectra which are directly observed, but are “demodulated”, to correct for the influence of the solar magnetosphere. At low particle energies the demodulation corrections are large, with large associated uncertainties.

Our results are shown in figure 3, in the form of heating rate per unit mass, as a function of the mean column-density, i.e. $\Gamma_0(\Sigma)$. Electron and proton contributions are shown separately (points) and in combination (solid line). Taken separately the electrons and protons display the same qualitative behaviour: at low columns the specific heating rate is approximately constant, while at high columns it declines according to

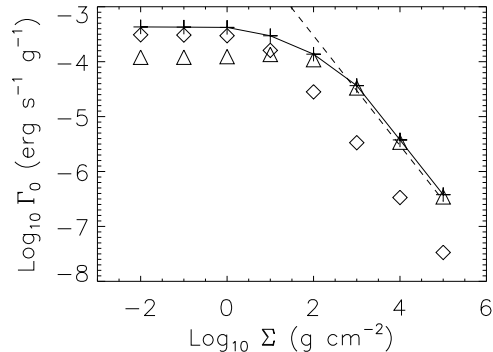


Fig. 3.— The cosmic-ray heating rate for dense gas clouds, as a function of the column-density of the cloud. The points are the results of computations with the GEANT Monte Carlo simulation package: diamonds show the electron contribution (primary cosmic-ray electrons of energy greater than 10 MeV); and triangles show the proton contribution (protons of energy greater than 100 MeV). The sum of these two components gives us the total heating rate shown by the crosses (connected with a solid line). The dashed line shows the limiting case, appropriate to very dense gas clouds, in which all of the incident cosmic-ray power is absorbed. The fact that the GEANT results lie slightly above this line, for high gas columns, is a reflection of energy non-conservation in hadronic interactions within GEANT.

$\Gamma_0 \propto \Sigma^{-1}$. For low column-densities our calculations yield cosmic-ray heating rates of order $3 \times 10^{-4} \text{ erg s}^{-1} \text{ g}^{-1}$ which are consistent with previously reported cosmic-ray ionisation rates appropriate to diffuse interstellar gas (e.g. Webber 1998), given an absorbed energy of approximately 7 eV per ionisation (Glassgold and Langer 1973; Cravens and Dalgarno 1978). However, we caution that our calculated heating rates in the low column-density regime are sensitive to the low-energy cutoff of the primary cosmic-ray electrons included in the simulation. More generally, this finding implies that at low column-density the heating rate is sensitive to the form of the adopted cosmic-ray electron spectrum at low energies, and in this regime the spectrum is poorly constrained. The uncertainties in cosmic-ray spectra have been highlighted by the recent determination (McCall et al 2003) of an ionisation rate, in a diffuse cloud (column $\sim 3 \times 10^{-3} \text{ g cm}^{-2}$), which is 40 times higher than previously assumed. This suggests that Γ_0 may be as large as $10^{-2} \text{ erg s}^{-1} \text{ g}^{-1}$ at the extreme left of figure 3. However, for the column densities which concern us here the heating rate is determined primarily by the total energy density in cosmic-rays (see below), and it is not clear whether the new data imply any significant

revision of this quantity.

The behaviour of the heating rate at high/low columns is straightforward to understand: for small columns the cloud is “optically thin” to the cosmic rays, so that the absorbed power is directly proportional to the mass of the cloud and the specific heating rate is independent of the column. At large columns essentially all of the power incident on the cloud surface is absorbed, so that the total heating rate is proportional to surface area, independent of the cloud mass, and the specific heating rate is therefore inversely proportional to the column-density. In this regime the computed heating rate is not sensitive to the details of the cosmic-ray spectrum, being dependent only on the total energy density resident in the cosmic rays. We are primarily interested in high column-density gas, for which the heating is mainly due to protons — most of the cosmic-ray energy-density being resident in protons of energy \sim few GeV. For our preferred column-density of $\Sigma \simeq 140 \text{ g cm}^{-2}$ (see §4.2), the heating rate is $\Gamma_0 \simeq 10^{-4} \text{ erg s}^{-1} \text{ g}^{-1}$; 80% of this power is contributed by the protons.

4.2. Properties of individual clouds

Individually the cloud mass and radius are poorly known, but the mean column-density, $\Sigma \equiv M_o/\pi R_o^2$, is quite tightly constrained because it determines the rate of conversion of dark to visible matter (W99). Matching the model to the Tully-Fisher relation for late-type spirals yields $\Sigma \simeq 140 \text{ g cm}^{-2}$ (W99). Essentially all of the uncertainty is then in the choice of cloud mass. The viable mass range is currently rather large, perhaps as broad as $10^{-6} M_\odot \lesssim M_o \lesssim 10^{-2} M_\odot$ (Wardle and Walker 1999). At present the best estimate we can make for the cloud mass comes from the optical variability of quasars: Hawkins (1993, 1996) pointed out that the observed optical variations, on a time-scale of years, could be interpreted in terms of a near-critical Universal density of planetary-mass gravitational lenses. In the context of our model, these lenses are to be identified with the individual gas clouds (whereas Hawkins[1993] suggested that they might be primordial black holes). Hawkins's (1993) estimate of the mass of the individual lenses is $10^{-3} M_\odot$. Schneider (1993), however, has modelled the same data set and his analysis suggests a mass of $10^{-4} M_\odot$ if the observed variability is interpreted as lensing. Minty (2001) re-examined this issue and demonstrated consistency between lensing models and the data for lens masses in the range $10^{-5} - 10^{-4} M_\odot$. The lower end of this range is, however, excluded by data on Galactic microlensing (Rafikov and Draine 2001), because of refraction in the neutral gas (Draine 1998). We adopt the value $10^{-4} M_\odot$. This choice then determines the cloud radius, because the column-density is fixed; correspondingly $R_o \simeq 1.4 \text{ AU}$, close to our adopted value (§4.1) of 1 AU.

The other key aspect of the individual clouds is their emission spectrum. The model of Wardle and Walker (1999), which focusses on the thermal stability of the clouds, requires that they be cooled by thermal continuum emission from H_2 precipitates. Here we assume, initially, that the hydrogen ‘‘snowflakes’’ are large compared to the $\sim \text{mm}$ wavelengths of their thermal emission, and that the individual snowflakes have a large optical depth to absorption at these wavelengths. These assumptions imply grey-body emission ($I_\nu \propto B_\nu$) at the temperature of the ‘‘snowflake’’. (Later, in §5, we will examine how

the model predictions are modified if we relax these assumptions.) The latter is, to a very good approximation, just the temperature of the atmosphere of the cloud. We noted earlier that the interior of the cloud is likely to be convective, and we can therefore make an estimate of the atmospheric temperature by calculating where an $n = 3/2$ polytropic model crosses the phase-equilibrium curve for hydrogen. Fixing the mean column density at $\Sigma = 140 \text{ g cm}^{-2}$, this method yields the following estimated atmospheric temperatures: 5.8, 4.9, 4.2, 3.7, 3.4 K, for clouds of mass $10^{-6}, 10^{-5}, 10^{-4}, 10^{-3}, 10^{-2} M_\odot$, respectively. For our preferred cloud mass, then, the atmospheric temperature is roughly 4.2 K, and this corresponds to a conversion factor of $\delta T/\delta I = 752 \text{ K erg}^{-1} \text{ s cm}^2 \text{ sr}$ between brightness-temperature, in the Rayleigh-Jeans limit, and bolometric intensity. In the formulation we have given, the root-mean-square intensity spectrum – i.e. the quantity $\delta I = \sqrt{l(l+1) C_l/2\pi}$ – has the units of bolometric intensity, and must be multiplied by this conversion factor to deduce the temperature anisotropy.

Similarly, when considering source counts, the conversion factor between flux density and bolometric flux for our model parameters is $F_\nu/F = 2.3 \times 10^{-16} \nu^2 \text{ Hz}^{-1}$, in the Rayleigh-Jeans regime, with ν in GHz. Using these conversion factors we can estimate the flux of the closest single cloud, it is $F_{max} \simeq 10 \text{ nKsr}$, implying that it may just be detectable by the MAP satellite (<http://map.gsfc.nasa.gov>). Sciama (2000a) has previously noted that the proposed Planck satellite (<http://astro.estec.esa.nl/Planck>) would easily detect the closest examples of the posited clouds. In more conventional units the expected flux of the brightest source can be written as $F_{max} \simeq 120 \text{ mJy}$ at 20 GHz, and scaling as ν^2 in the Rayleigh-Jeans regime ($\nu \ll 150 \text{ GHz}$).

4.3. Properties of the minihalos

The mass-spectrum of the mini-halos is given in equation 12, but we have not yet specified the range $[M_1, M_2]$ over which it applies. It is implicit in equation 12 that the (dark) density ρ is entirely composed of mini-halos with masses in the range $M_1 < M < M_2$. The appropriate value of M_1 is difficult to estimate. To form a stable cluster there should be a large number of clouds in each

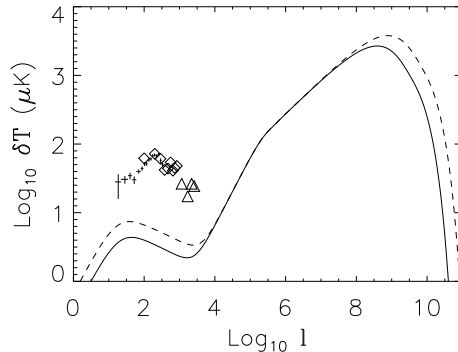


Fig. 4.— Microwave anisotropy spectra due to emission from cold, Galactic clouds. This plot shows the root-mean-square brightness-temperature fluctuations, $\delta T = [l(l+1)(C_l^u + C_l^c)/2\pi]^{1/2}$, as a function of spherical harmonic index, l , in the Rayleigh-Jeans limit. The large peak at $l \sim 3 \times 10^8$ is the Poisson noise from individual clouds, while the smaller peak at lower l is due to bound clusters of clouds (mini-halos) with an assumed CDM-like mass spectrum. The figure shows the predicted spectrum appropriate to a small area of sky ($\Delta\Omega \sim 0.1$ sr) at high/low Galactic latitude (solid/dashed lines: $|b| = 90^\circ/|b| = 30^\circ$ respectively), and data taken at high latitude with the DASI instrument (diamonds; Pryke et al 2002), and the CBI (triangles; Mason et al 2002). Also shown on this panel are the results from Archeops (crosses; Benoît et al 2002), based on data covering an area $\Delta\Omega \simeq 1$ sr above $b = 30^\circ$.

mini-halo, although the choice of what constitutes a large number is somewhat arbitrary; we have chosen $M_1 = 0.1 M_\odot \sim 10^3 M_o$. The upper limit is easier to estimate: M_2 should be chosen such that there is a 50% chance of finding a more massive halo within the field-of-view. If the total mass of the dark halo of our Galaxy is M_{tot} , which we take to be $2 \times 10^{12} M_\odot$ (Zaritsky 1999), then it follows that

$$\frac{1}{2} \sim \frac{\Delta\Omega}{4\pi} \frac{M_{tot}}{M_2 \log_e(M_2/M_1)}, \quad (23)$$

and solving yields $M_2 \simeq 1.4 \times 10^9 M_\odot$ for $\Delta\Omega = 0.1$ sr. Fortunately our final results are not very sensitive to the particular values of $M_{1,2}$ adopted, as they enter principally through the factor $\log_e(M_2/M_1) \simeq 23$, and secondarily through the limits of integration ($z_{1,2} \propto M_{1,2}^{1/3}$).

4.4. Temperature anisotropies and constraints

With the above numerical estimates, and the power-spectrum formulations derived in §§2,3, we are now in a position to quantify the temperature anisotropies expected in the present model. The results are graphed in figure 4, showing both the

mini-halo contribution, which leads to the peak at $l \sim 50$, and the much larger peak at $l \sim 3 \times 10^8$ is the Poisson noise from individual clouds.

Recalling, from §2.2, that the mean sky brightness is approximately $30 \mu\text{K}$, in our model, we see that the mini-halos introduce fluctuations which are small in comparison with the mean intensity, while the reverse is true for the fluctuations due to the individual clouds. This difference simply reflects the fact that the mini-halos are sufficiently large that they cover the entire sky several times over, whereas the individual clouds cover only a tiny fraction of the sky and the root-mean-square intensity is consequently much greater than the mean. It is worth emphasising that each of these contributions is computed under the assumption that *all* of the dark matter is in the corresponding form – i.e. clustered into mini-halos, or entirely unclustered – and the calculated contributions are in this sense mutually exclusive. However, recognising that (i) the minihalos are made up of individual clouds, (ii) the minihalos are unbiased tracers of the mean density, and (iii) the minihalos introduce only a small modulation around the mean sky brightness, we see that in practice the predicted properties of the \sim milli-arcsecond fluc-

tuation peak are largely independent of whether or not the clouds are clustered into minihalos. If all the clouds are clustered into minihalos, then there would, however, be many fewer clouds very local to the Sun, and so the low-frequency (i.e. small l) power from individual clouds would be much reduced.

How do our predictions compare with existing data? We do not consider, here, the low-order multipoles ($l \lesssim 10$) which were measured by COBE (Smoot et al 1992), because the calculations we have undertaken are valid only for $l \gg 1$. The COBE detections at small l did, however, create great interest in measuring the higher order multipoles, and after much effort expended on special-purpose experiments there are now several clear detections of anisotropies on degree scales (e.g. de Bernardis et al 2000; Hanany et al 2000; Pryke et al 2002; Benoît et al 2002). The peak of the observed signal – $\delta T_b \simeq 70 \mu\text{K}$ at $l \simeq 200$ – is roughly 20 times larger than the model predictions at the same angular scale, for high-latitude fields, and for many purposes this small contribution to the observed power (about 0.3%) can be neglected. However, it may still be possible to detect the predicted mini-halo anisotropies against the background of the dominant CMB fluctuations, if we select the data appropriately. In particular the CMB anisotropies fall to $\simeq 30 \mu\text{K}$ at multipoles $l \sim 50$, near the peak of the predicted spectrum, while the latter attains a value $\simeq 8 \mu\text{K}$ at $|b| = 30^\circ$. Data collected by the MAP satellite¹ should be able to reveal this Galactic foreground, provided that the spectrum is close to the assumed grey-body form (see §5 and figure 5).

To date there has been only limited interest in the arcminute-scale anisotropies, because Silk damping is expected to strongly suppress any primary cosmological anisotropy on these scales (Silk 1968). Consequently there is at present only a limited amount of data in the region $10^3 \lesssim l \lesssim 10^4$ (Subrahmanyan et al 1997; Dawson et al 2001; Mason et al 2002). Here again the observed signal is large in comparison with the model: $25 \mu\text{K}$ at $l \sim 2500$ (Mason et al 2002); roughly an order of magnitude larger than the anisotropies predicted by the present model. Consequently data at these very high multipoles do not yet provide strong con-

straints on the model we have presented. Moreover these angular scales are below the resolution of the instrumentation carried by MAP, so there is no immediate prospect of a major improvement in sensitivity. It would, however, be useful to obtain further measurements of the power-spectrum using ground-based interferometers, particularly with a view to constraining its latitude dependence, because the origin of the observed high-frequency power (Mason et al 2002) is not clear at present and it remains possible that it is a Galactic signal.

For $l \gg 10^4$ the anisotropies predicted by our model are dominated by the individual clouds, and more specifically the closest examples within the area under study; consequently for these angular scales the model predicts very little latitude dependence in the power-spectrum. The domain of large l is also technically challenging, in that the sensitivity of an interferometer to surface brightness fluctuations worsens in proportion to l . Thus the predicted milli-Kelvin peak on milli-arcsecond scales is not immediately open to experimental scrutiny. Fortunately the model predictions can be put to the test in another way: rather than attempting to measure the anisotropies per se we can simply study the bright source counts. At low frequencies the flux from each cloud increases as ν^2 , or faster, whereas the flux from non-thermal (synchrotron) radio sources typically declines with increasing frequency. Thus in a sky-survey for compact sources at high frequencies the predicted population should stand out. For the purposes of testing the model, the ideal approach is to make a survey of a large fraction of the sky, with sufficient sensitivity to detect sources having flux much less than F_{max} . The model then predicts that many sources with thermal spectra should be detected, and any such sources can be selected out and subjected to detailed studies to determine their nature.

To date surveys at high radio frequencies have covered only a very small fraction of the sky with the necessary sensitivity — this is simply a consequence of the rapid decrease in area of the primary beam of an antenna, as the observing frequency increases, requiring a much larger number of pointings to cover a given area of sky. For example, the survey of Taylor et al (2001), made with the Ryle Telescope, covered only 63 deg^2 at

¹<http://map.gsfc.nasa.gov>

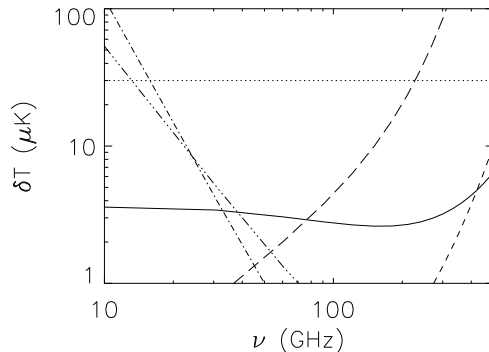


Fig. 5.— Frequency dependence of the root-mean-square temperature anisotropies at Galactic latitude $|b| = 90^\circ$ and multipole $l \simeq 50$, for various processes. The curves shown here are for: the microwave background anisotropies (dotted line; $T = 2.73$ K, and $\delta T_b = 30 \mu\text{K}$); mini-halo anisotropies for a grey-body spectrum at $T = 4.2$ K (solid line); mini-halo anisotropies for a “dusty” spectrum (i.e. $I_\nu \propto \nu^4$ at low frequencies) at $T = 4.9$ K (short-dashed line); emission from dust ($T = 21$ K) in the diffuse interstellar medium (long-dashed line); synchrotron emission (dot-dashed line); and free-free emission (dot-dot-dashed line). The last three of these are taken from Tegmark and Efstathiou (1996).

$\nu = 15$ GHz, to a flux limit of 20 mJy. Using the predicted source-counts for our model (§§2.1,4.2), it is straightforward to estimate that the expected number of cloud detections for this survey is approximately 0.01 and these data therefore have little to say about the present model. A more extensive interferometric survey, covering the entire southern sky, is planned for later this year. This survey is expected to have a flux limit of roughly 40 mJy at 20 GHz – thus improving substantially on the pilot survey (Ekers et al 2003) – and could detect examples of the closest clouds if their spectra are indeed grey bodies (see §5).

Deep surveys at much higher frequencies have also been undertaken, again covering very small areas of the sky. Interestingly, Lawrence (2001) has pointed out that the “blank field SCUBA sources” are consistent with being a very local population of Galactic sources, rather than high-redshift star-forming galaxies as is usually assumed. Indeed Lawrence (2001) points out that their properties are remarkably similar to those expected for the population of cold gas clouds postulated by Walker and Wardle (1998); the main point of discrepancy noted by Lawrence is that he infers a thin disk population, rather than a quasi-spherical halo. However, as noted earlier, the luminosity of each cloud is determined by the

cosmic-ray heating rate, and models of the Galactic synchrotron emission (Higdon 1979; Beuermann Kanbach and Berkhuijsen 1985) suggest that the cosmic-ray energy density initially declines very rapidly (scale-height ~ 0.3 kpc) as one moves away from the plane of the disk, changing to a more gradual decline further out. Thus the discrepancy suggested by Lawrence might not be all that serious. Clearly problematic, though, in the context of the present model, is the high bolometric flux of the SCUBA sources. For a 2 mJy source density of 10^3 deg^{-2} – as per Lawrence (2000) – assuming Euclidean source counts, the brightest source on the sky should be of order 240 Jy. These are continuum fluxes at $850 \mu\text{m}$ (3.5×10^{11} Hz), so the bolometric flux of the brightest source should be of order $10^{-9} \text{ erg cm}^{-2} \text{ s}^{-1}$. The present model predicts a maximum bolometric flux (§2.1) which is only 1% of this value, based on cosmic-ray heating. This conclusion is largely independent of the spectrum of the emission, within the plausible range of possibilities. However, it is important to note that Lawrence’s analysis excluded grey-body spectra for the SCUBA sources, preferring a “dusty” thermal emission spectrum (see next section). Lawrence’s interpretation of the SCUBA data can be tested by surveying a large area of the sky, in order to measure the bright source

counts, and following up with detailed studies of the brightest (presumably the closest) sources. The Planck satellite² should be able to detect the closest of the individual dense gas clouds (Sciamia 2000a).

5. Discussion

The calculations presented in §4.4 assume that the cold gas emits as a grey-body. This is plausible, but not certain. Lawrence (2001) has suggested that the Blank Field SCUBA sources are cold, dense gas clouds, with properties similar to those which we have considered in this paper, and he uses data on these sources to *exclude* grey-body spectra, preferring “dusty” spectra which exhibit much less flux at frequencies below the thermal peak. In addition to this uncertainty, the atmospheric temperature could be slightly higher than the 4.2 K we have adopted, again diminishing the predicted power at low frequencies. We have quantified these uncertainties by computing the mini-halo anisotropies for two models representing the plausible range of emitted spectra: a 4.2 K grey-body spectrum (the reference model used in the foregoing sections of the present paper), and a 4.9 K “dusty” spectrum (i.e. $I_\nu \propto \nu^4$ at low frequencies). The results are shown in figure 5 for the $l \simeq 50$ peak of the model anisotropies, together with models (adapted from Tegmark and Efstathiou 1996) for the known Galactic foregrounds (diffusely distributed dust, synchrotron and free-free emission). The plot is made for $|b| = 90^\circ$, and at lower latitudes all of the Galactic contributions scale up as $1/|\sin b|$.

From this figure we can see that, in the case of a grey-body spectrum, mini-halo anisotropies are predicted to be the dominant Galactic foreground for observing frequencies in the range 40–80 GHz, at multipoles $l \sim 50$. Furthermore, the predicted power contribution amounts to $\sim 5\%$ of the cosmic background anisotropies, at $|b| = 30^\circ$ and may therefore be detectable with data from the MAP satellite. On the other hand, if the emission spectrum of the clouds is “dusty” we can see that the predicted mini-halo anisotropies are negligibly small at all frequencies, and could not expect to be detected by any current or planned instrument.

The foregoing considerations are specific to the anisotropy power spectrum, but it may be possible to detect microwave emission from the mini-halos in other ways. In particular we note that the brightest mini-halos may be detectable as individual sources. In this case those sources should also be bright in gamma-rays, and a sensible strategy is therefore to search for microwave counterparts to the Unidentified EGRET sources (Walker, Mori and Ohishi 2003). We also note the possibility of detecting the predicted microwave foreground component via its mean intensity which, as noted earlier, is much larger than the anisotropy level. For grey-body emission the mean intensity is roughly $30/|\sin b| \mu\text{K}$ in the Rayleigh-Jeans regime.

The fact that the present model naturally yields a degree-scale anisotropy peak, in the form of low-temperature thermal radiation, suggests that it might be possible to construct a model in which the observed microwave anisotropies are interpreted entirely in terms of emission from mini-halos. In support of this idea we note that (i) the frequency dependence of the anisotropies would be quite small (assuming a grey-body spectrum at 4.2 K – see figure 5), and (ii) the heating rate of the clouds might be rather larger than our estimate, either because of a very large population of low-energy cosmic-rays (see the discussion in §4.1), or because there are other heat sources which are more important than cosmic-rays. However, a generic prediction of any such model is a strong latitude dependence of the peak power, and this is at odds with existing constraints on any latitude dependence (Griffiths and Lineweaver 2003).

6. Conclusions

We have calculated the microwave anisotropies which are expected in a model where the dark halo of the Galaxy is composed entirely of cold, dense gas clouds, heated by cosmic-rays. There are contributions to the anisotropy arising from the Poisson noise of individual clouds, and from the Poisson noise of clusters of clouds. The latter contribution has been computed under the assumption of a CDM-like mass-spectrum for the clustering, and we find that it peaks at $l \sim 50$. The Poisson noise contributed by individual clouds is, for $l \ll 3 \times 10^8$, isotropic and sufficiently small that

²<http://sci.esa.int/home/planck>

it will be extremely difficult to detect. A better approach to constraining this component is to attempt to detect the individual clouds themselves, and this is best done with high-resolution all-sky surveys at high frequencies. The Planck satellite will collect data of this type and should detect $\gtrsim 10$ such sources.

The predicted power due to clusters of clouds increases toward the Galactic plane as $1/\sin^2 b$. If the clouds emit as grey-bodies, then such clusters are predicted to be the dominant Galactic foreground over the range 40–80 GHz, at multipoles $l \sim 50$. For these circumstances the predicted power contribution is $\sim 5\%$ at $|b| = 30^\circ$, and by virtue of its latitude dependence this component may be detectable in MAP data. On the other hand, if the clouds have a “dusty” emission spectrum, then their contribution to the anisotropies is too small to be detected, being swamped by other Galactic foregrounds at all frequencies.

We thank Mark Wardle for providing his radial temperature profile for a polytrope with index $n = 3/2$, and Lister Staveley-Smith for a critical reading of the manuscript.

REFERENCES

- Benoît A. et al 2002 *astro-ph/0210305*
- Beuermann K., Kanbach G., Berkhuijsen E.M. 1985 *A&A* 153, 17
- Binney J., Tremaine S. 1987 “Galactic Dynamics” (PUP, Princeton)
- Blumenthal G., Faber S.M., Primack J.R., Rees M.J. 1984 *Nature* 311, 527
- Cravens T.E., Dalgarno A. 1978 *ApJ* 219, 750
- Davis M., Efstathiou G., Frenk C.S., White S.D.M. 1985 *ApJ* 292, 371
- Dawson K.S., Holzapfel W.L., Carlstrom J.E., Joy M., LaRoque S.J., Reese E.D. 2001 *ApJL* 553, L1
- de Bernardis P. et al 2000 *Nature* 404, 955
- de Oliveira-Costa A., Tegmark M. 1999 “Microwave Foregrounds” (ASP, San Francisco)
- De Paolis F., Ingrassio G., Jetzer Ph., Roncadelli M. 1995, *A&A*, 295, 567
- Draine B.T. 1998 *ApJL* 509, L41
- Ekers R.D. et al 2003 In preparation
- Fiedler R., Dennison B., Johnston K.J., Hewish A. 1987 *Nature* 326, 675
- Fiedler R., Dennison B., Johnston K.J., Waltman E.B., Simon R.S. 1994 *ApJ* 430, 581
- Gerhard O., Silk J. 1996, *ApJ*, 472, 34
- Ghigna S., Moore B., Governato F., Lake G., Quinn T., Stadel J. 1998 *MNRAS* 300, 146
- Glassgold A.E., Langer W.D. 1973 *ApJ* 186, 859
- Griffiths L.M., Lineweaver C.H. 2003 *ApJ*, Submitted (*astro-ph/0301490*)
- Hanany S. et al 2000 *ApJL* 545, L5
- Hawkins M.R.S. 1993 *Nat* 366, 242
- Hawkins M.R.S. 1996 *MNRAS* 278, 787
- Henriksen R.N., Widrow L.M. 1995, *ApJ*, 441, 70
- Higdon J.C. 1979 *ApJ* 232, 113
- Hogan C.J. 1993 *ApJL* 415, L63
- Hu W., Dodelson S. 2002, *ARAA* (In press); *astro-ph/0110414*
- Klypin A., Kravtsov A.V., Valenzuela O., Prada F. 1999 *ApJ* 522, 82
- Kogut A. et al 1996 *ApJL* 464, L5
- Lawrence A. 2001 *MNRAS* 323, 147
- McCall B.J. et al 2003 *Nature* (in press; *astro-ph/0302106*)
- Mason B. et al 2002 *ApJ* (submitted; *astro-ph/0205384*)
- Minty E.M. 2001 PhD Thesis, University of Edinburgh
- Moore B., Ghigna S., Governato F., Lake G., Quinn T., Stadel J., Tozzi P. 1999 *ApJL* 524, L19
- Mori M. 1997 *ApJ* 478, 225
- Ohishi M., Mori M, Walker M.A. 2003 (In preparation)
- Peebles P.J.E. 1992 “Principles of Physical Cosmology” (PUP, Princeton)
- Pfenniger D., Combes F., Martinet L. 1994, *A&A*, 285, 79
- Pryke C., Halverson N.W., Leitch E.M., Kovac J., Carlstrom J.E., Holzapfel W.L., Dragovan M. 2002 *ApJ* 568, 46

Rafikov R.R., Draine B.T. 2001 ApJ 547, 207
Schneider P. 1993 A&A 279, 1
Sciama D. 2000a MNRAS 312, 33
Sciama D. 2000b MNRAS 319, 1001
Silk J. 1968 ApJ 151, 459
Skibo J., Ramaty R. 1993 A&AS 97, 145
Smoot G. et al 1992 ApJL 396, L1
Subrahmanyan R., Kesteven M.J., Ekers R.D.,
Sinclair M., Silk K. 2000 MNRAS 315, 808
Taylor A. et al 2001 MNRAS 327, L1
Tegmark M., Efstathiou G. 1996 MNRAS 281,
1297
Toffolatti L., De Zotti G., Argüeso F., Burigana C.
1999 ASP Conf. Ser. 181, 153
Turner M.S., Tyson J.A. 1999 RModPhys 71, S145
Umebayashi T., Nakano T. 1981 PASJ 33, 617
Walker M. 1999 MNRAS 308, 551 (W99)
Walker M.A., Mori M., Ohishi M. 2003 ApJ In
press (astro-ph/0212572)
Walker M., Wardle M. 1998 ApJ 498, L125
Walker M., Wardle M. 1999 PASA 16, 262
Wardle M., Walker M. 1999 ApJL 527, L109
Webber W.R. 1998 ApJ 506, 329
Webber W., Lee M., Gupta M. 1992 ApJ 390, 96
Zaritsky D. 1999 ASP Conf. Ser 165, 34